LBL-21215
Preprint

Lawrence Berkeley Laboratory
UNIVERSITY OF CALIFORNIA

Accelerator & Fusion
Research Division

Submitted to Particle Accelerators

STUDY OF FODO STRUCTURES FOR A SYNCHROTRON LIGHT SOURCE

A. Wrulich

July 1986

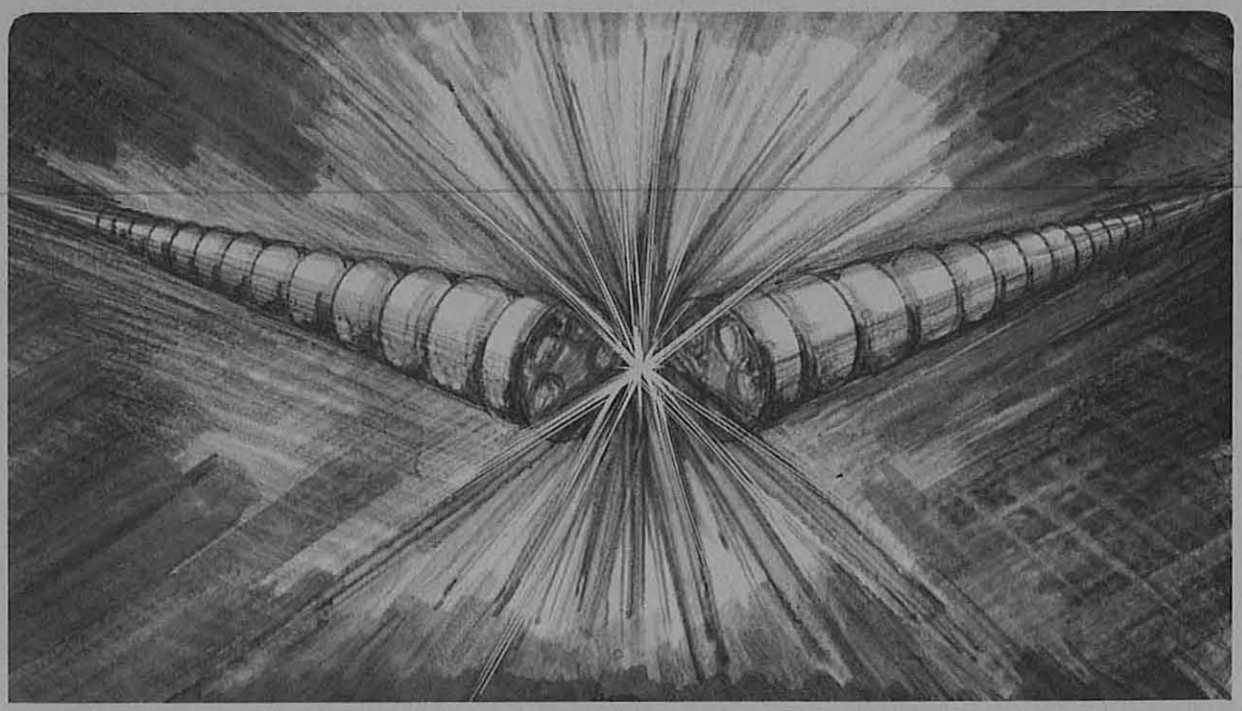

Prepared for the U.S. Department of Energy under Contract DE-AC03-76SF00098

LBL-21215
ESG-9

STUDY OF FODO STRUCTURES FOR A SYNCHROTRON LIGHT SOURCE*

A. Wrulich

Lawrence Berkeley Laboratory
University of California
Berkeley, CA 94720

July 1986

*This was supported by the Director, Office of Energy Research, Office of High Energy and Nuclear Physics, High Energy Physics Division, U.S. Dept. of Energy, under Contract No. DE-AC03-76SF00098.

STUDY OF FODO STRUCTURES FOR A SYNCHROTRON LIGHT SOURCE*

A. Wrulich

*This was supported by the Director, Office of Energy Research, Office of High Energy and Nuclear Physics, High Energy Physics Division, U.S. Dept. of Energy, under Contract No. DE-AC03-76SF00098.

I. Introduction

Synchrotron radiation is a helpful tool to investigate a wide range of physical, chemical and biological phenomena. Extremely high flux, brilliance synchrotron radiation can be achieved in low emittance electron storage rings with wigglers and undulators.

The Advanced Light Source (ALS) is a synchrotron radiation source with 1.5 GeV design energy [1]. The lattice is designed with 12 superperiods each containing a 6 m long straight section to accomodate the insertion devices. Two straight sections are reserved for injection elements and accelerating cavities. To minimize source width and angular divergence the dispersion is matched to zero in the straight sections.

The goals for the design of such a lattice are low emittance, flexibility and large dynamic apertures after chromaticity correction, at low cost. The most economical, and therefore most frequently used structure in the past is that suggested by Chasman and Green [2].

It has become apparent recently that alternative designs with excellent characteristics have been proposed for synchrotron light sources. Therefore a new lattice design study for the ALS has been carried out. The Triple Bend Achromat (TBA) lattice proposed by Vignola [3] has been compared with the Chasman-Green lattice [4]. An expanded Chasman-Green lattice proposed by Hutton [5] was reviewed for the ALS [6]. Finally the FODO achromat lattice as proposed by Wiedemann for the SSRL [7] has been studied as a candidate for the ALS.

The results for the FODO achromat lattice are presented here. In part II the minimum emittance of the FODO achromat has been derived in a semianalytical approach. It has been shown, that after performing two optimization steps, the emittance can be reduced far below the minimum emittance of a pure FODO structure.

In part III, three examples of the FODO achromat lattices for the ALS are presented. For the relatively short structure of the ALS, the minimum emittance

unfortunately cannot be utilized because the strong focusing produces large chromatic aberrations which must be compensated with sextupoles of high strengths. These sextupoles generate geometric aberrations which reduce the dynamic acceptance below the acceptable limit. Therefore the FODO structures presented in part III are a compromise between the conflicting requirements of small emittance and large dynamic acceptance.

II. Minimum Emittance of a FODO Achromat

In electron rings the natural emittance is given by the equilibrium between quantum excitation and radiation damping. In an undistorted machine quantized radiation occurs mainly in the normal bending magnets. Due to the emission of a quantum the particle looses energy and therefore the corresponding closed orbit is changed and betatron oscillations are excited. The average beam size produced by this excitation in equilibrium to the radiation damping can be described by the emittance

$$\varepsilon_x = C_0 \frac{\gamma^2 \left\langle \left| \frac{1}{\rho^3} \right| \varepsilon_D \right\rangle}{J_x \left\langle \frac{1}{\rho^2} \right\rangle} \qquad (1)$$

with

$$C_0 = \frac{55}{32\sqrt{3}} \frac{\hbar}{mc}$$

$$\varepsilon_D = D'^2\beta + 2D'D\alpha + D^2\gamma$$

ρ bending radius

γ Lorentz factor $= E/m_0c$

J_x damping partition number, which in an isomagnetic system as the FODO structure is approximately 1.0

For a single magnet with length L and $\rho = \text{const}$, the integral for deriving the average value of the numerator in (1) is given by

$$I = \int_0^L \left(D'^2\beta + 2\alpha DD' + D^2\gamma\right) ds$$

$$= \left(D_0'^2\beta_0 + 2D_0D_0'\alpha_0 + D_0^2\gamma_0\right) L + 2\left(D_0\alpha_0 + D_0'\beta_0\right)\rho\left(L - \cos\frac{L}{\rho}\right)$$

$$- 2\left(D_0\gamma_0 + D_0'\alpha_0\right)\rho\left(L - \rho\sin\frac{L}{\rho}\right)$$

$$+ \frac{\beta_0}{2}\left(L - \frac{\rho}{2}\sin\frac{2}{\rho}L\right) - 2\alpha_0\rho^2\left(\frac{3}{4} - \cos\frac{L}{\rho} + \frac{1}{4}\cos\frac{2}{\rho}L\right)$$

$$+ \gamma_0\rho^2\left(\frac{3}{2}L - 2\rho\sin\frac{L}{\rho} + \frac{\rho}{4}\sin\frac{2}{\rho}L\right) \qquad (3)$$

where a sector bending magnet has been used for the derivation of the expression and the index "0" denotes values at the entrance to the magnet. Equation (4) can be simplified by approximating the expression up to 2nd order in L/ρ resulting in

$$I \approx \left(D_0'^2\beta_0 + 2D_0'D_0\alpha_0 + D_0^2\gamma_0\right) L + \left(D_0\alpha_0 + D_0'\beta_0\right)\frac{L^2}{\rho} - \left(D_0\gamma_0 + D_0'\alpha_0\right)\frac{L^3}{3\rho}$$

$$+ \left(\beta_0\frac{L}{3} - \alpha_0\frac{L^2}{4} + \gamma_0\frac{L^3}{20}\right)\frac{L^2}{\rho^2} \qquad (4)$$

The emittance of a FODO achromat is essentially produced in the two different sections sketched in the following figure. The total emittance is obtained by summing these values over the various bending magnets in the lattice.

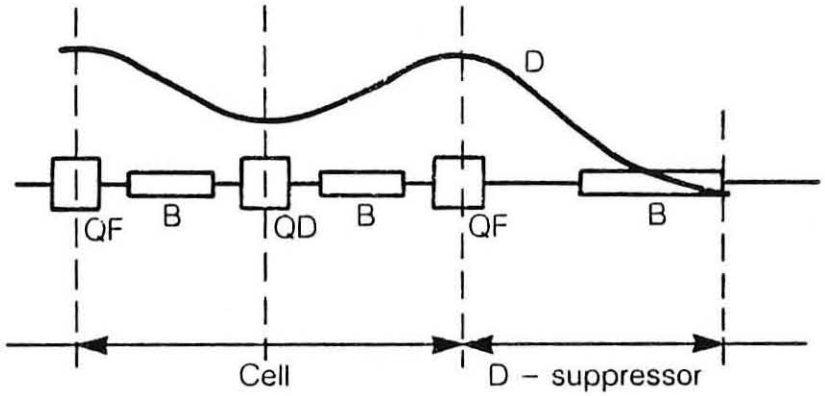

XBL 865-10809

The regular FODO structure is followed by a dispersion suppressor. Thus the natural emittance produced by these two types of magnets can be expressed in the following form:

$$\varepsilon_x = C_0 \frac{\gamma^2}{J_x} \frac{\frac{n_0 I_0}{\rho_0^3} + \frac{2I_1}{\rho^3}}{\frac{n_0 \varphi_0}{\rho_0} + \frac{2\varphi_1}{\rho}} \qquad (5)$$

with n = number of FODO half cells per achromat

$$\varphi = \frac{L}{\rho} \qquad (6)$$

As an example, two extreme cases will be considered. A structure consisting of regular FODO cells only and a Chasman - Green achromat built up of only two symmetrically arranged dispersion suppressor magnets with a quadrupole in between

Pure FODO structure:

In the thin magnet approximation the dispersion in the middle of 2 quadrupoles in the half cell is given by

$$D = \frac{\varphi_0 f^2}{\ell}\left(\ell - \frac{\ell^2}{4f^2}\right)$$

$$D' = -\frac{\varphi_0 f}{\ell} \qquad (7)$$

with f focal length of the half cell quadrupole

l length of the half cell

The emittance produced by the bending magnet is dominated by the first term in Eq. (4). For a pointlike bending magnet in the middle of the two cell quadrupoles it is approximately given by

$$\varepsilon_x = C_0 \gamma^2 \frac{4\varphi_0^3 f^3}{L\ell^2} \qquad (8)$$

With the assumption that the bending magnet length scales with the cell length, i.e.

$L = r.l$ and $l/f = \sin(\phi) = \text{const.}$ ϕ phase advance per half cell

the emittance becomes

$$\varepsilon_x = C_0 \gamma^2 \frac{4\varphi_0^3}{r(\sin\phi)^3}$$

Equation (9) shows that there are two ways to reduce the emittance. Either to increase the phase advance per cell, or to reduce the bending angle. Note that the expression is independent of the cell length. Thus, the emittance can be reduced by decreasing the cell length (and keeping the phase advance per cell constant) until to the technical limitation. After reaching the technical limitation it can only be further reduced by adding more cells, i.e. by reducing the bending angle.

Chasman-Green achromat:

Since the dispersion and its derivative are zero at the appropriate entrance of the dispersion suppressor magnet, only the last term in Eq. (4) is nonvanishing, i.e. the emittance is given by

$$\epsilon_x = C_0 \gamma^2 \frac{\varphi^3}{\rho} \left(\frac{1}{3} \beta_0 - \frac{L}{4} \alpha_0 + \frac{L^2}{20} \gamma_0 \right) \tag{10}$$

After optimizing this expression consecutively with regard to β_0 and α_0 we get the minimum emittance

$$\epsilon_x = C_0 \gamma^2 \frac{\varphi^3}{4\sqrt{15}} \tag{11}$$

for the following optical parameters at the entrance of the bending magnet

$$\beta_0 = 2L \sqrt{\frac{3}{5}}, \quad \alpha_0 = \sqrt{15} \tag{12}$$

The minimum of the beta value within the bending magnet occurs at the distance s_0 from the entrance of the magnet, given by

$$s_0 = \frac{3}{8} L \qquad (13)$$

To achieve the minimum emittance of the FODO achromat, as pointed out above, the parameters of the FOFO cells should be chosen close to the technical limitations concerning magnet spacing and field strengths of bending magnet and quadrupole. The drift length between quadrupole and bending magnet must provide enough space for the sextupole. Since the required sextupole length (i.e. strength) is not known a priori, empirical values must be taken which can then be modified if necessary in a second iteration step.

For the subsequent optimizations the following geometry of the FODO - half cell has been used:

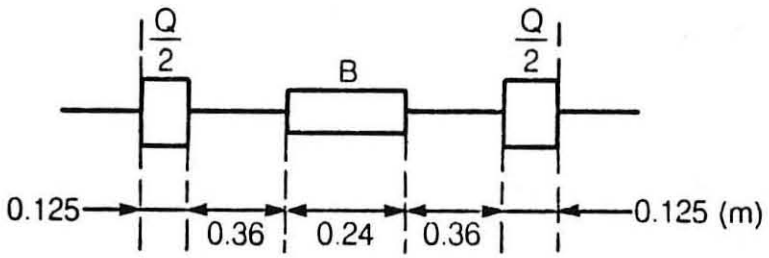

XBL 865-10810

(which fits the requirement for the ALS).

As has been shown in Eq. (9), the phase advance of the cell should be chosen as larg as possible to achieve the minimum emittance. On the other hand the strength of the sextupoles (which are necessarily introduced to compensate the natural chromaticity but also cause undesired nonlinear effects) increase considerably with increasing phase advance. The sextupole strengths for zero chromaticity are given by the following equation

$$S_{F,D} = \frac{1}{D_{F,D}} \left\{ \frac{1}{f} + \frac{4\pi(\xi_x \hat{\beta}_c + \xi_z \check{\beta}_c)}{N_c\left(\hat{\beta}_c^2 - \check{\beta}_c^2\right)} \right\} \qquad (14)$$

The first term in the braces is generated by the cell chromaticity, whereas the second term is generated by the chromaticities produced outside of the FODO structure and which are also compensated by the sextupoles within the FODO structure. For increasing cell phase advance the sextupole strength increases with the cube of the focal length, since the dispersion increases quadratically with the focal length. For the present considerations a cell phase advance of 90 degrees has been assumed (this does not affect the principle of the optimization procedure).

Once the geometry of the cell and the phase advance are defined, the optical properties of the cell are given. The minimization of the emittance can then be performed in two steps:

1. Optimization of the dispersion suppressor

The bending angles of FODO magnet and dispersion suppressor magnet are related by the requirement that the overall deflection must be 2π i.e.

$$n\varphi_0 + 2\varphi_1 = \frac{2\pi}{p} \qquad (15)$$

with n number of FODO half cells

p number of achromats in the ring

φ_0, φ_1 bending angles of FODO magnet and dispersion suppressor magnet respectively

To suppress the dispersion, the slope of the dispersion at the end of the FODO structure must be adjusted to

$$D' = - \sin(\varphi_1)$$

As indicated in the following sketch. To produce the required dispersion slope focusing must be added beyond the symmetry point of the last FODO cell

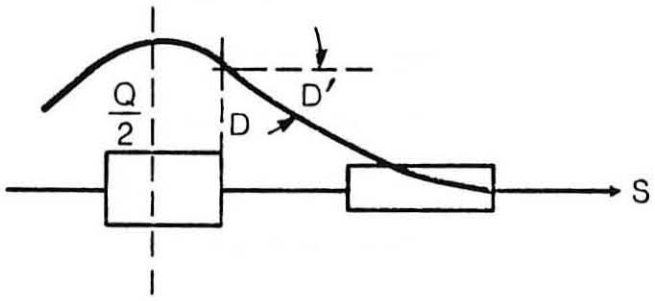

XBL 865-10808

Note: $D'(d+L/2) = -D$

The emittance contribution of the dispersion suppressor magnet as defined in Eq. (4) can be expressed by the optical parameters of the FODO - cell and the properties of the dispersion suppressor magnet.

$$\left\langle \left| \frac{1}{\rho^3} \right| \epsilon_D \right\rangle = \frac{1}{L_1 \rho_1^3} I_1 = \frac{\varphi_1^2}{3\rho_1^3} \left\{ \tilde{\beta} - \frac{L_1}{4} \tilde{\alpha} + \frac{L_1^2}{40} \tilde{\gamma} \right\}$$

with

$$\tilde{\beta} = \beta_0 - 2\tilde{d}\alpha_0 + \gamma_0 \tilde{d}^2 \qquad (16)$$

$$\tilde{\alpha} = \alpha_0 - \gamma_0 \tilde{d}$$

$$\tilde{\gamma} = \gamma_0$$

$$\tilde{d} = \left(\frac{D_0}{\varphi_1}\right) \quad \beta_0, \alpha_0, \gamma_0, D_0 \quad \text{cell parameters}$$

The length of the dispersion suppressor magnet can now be adjusted to minimize the overall emittance of the FODO achromat, as given by Eq. (5). Figure 1 shows the variation of emittance with magnet length for two different bending angle distributions. In the first case the bending angle of the dispersion suppressor magnet has been chosen equal to the FODO magnet, in the second case it was twice as large. In both cases it has been assumed, that there are four half cells per achromat.

2. Optimization of the bending angle distribution

It has been demonstrated by the examples shown above, that for equal bending angles of the two magnet types the emittance generated in the dispersion suppressor magnet is much less than that generated in the FODO magnet. For constant overall bending angle as defined in Eq. (15), the bending angle distribution can now be varied to minimize the the emittance defined by Eqs. (5) and (32). Figures 2 and 3 show the emittance variations as a function of FODO bending angle. Different curves correspond to different machine designs, i.e. different numbers of half cells and achromats per ring. For every bending angle distribution the dispersion suppression has been optimized as described for in the 1st optimization step. Note that the ratio of the angles for the minimum emittance is independent of the number of half cells and achromats per period once the geometry and phase advance of the cell are fixed. For the present example the ratio is :

$$\frac{\varphi_1}{\varphi_0} \approx 4.26$$

The boundary of the curves to the left side is given by the technical limitation of the dispersion suppressor magnet. If φ_0 is decreasing, φ_1 is correspondingly increasing, that means the strength of the dispersion suppressor magnet becomes larger. In addition the central deflection point of the bending magnet is moving closer to the quadrupole. For increasing φ_0 the maximum is achieved if all the bending is performed by the FODO magnets only.

For most of the cases with practical relevance for the ALS the sextupole strengths of the minimum emittance optics are considerably reducing the dynamical aperture. To increase the acceptance, i.e. to reduce the sextupole strengths one can proceed two different ways (in both cases of course the emittance is increased again):

i. By increasing the FODO bending angle and moving out of the minimum emittance range. This reduces the sextupole strength like as given by Eqs. (7) and (14) inversely proportional to the bending angle φ_0, or

ii. By increasing the cell length, which reduces the sextupole strength like the square of the cell length. In this case the beta values increase proportionally with the cell length enhancing also the higher order geometric aberrations.

II. ALS FODO - Structures

The optimization procedure outlined in the previous chapter has been adopted for the development of various example FODO achromat structures for the ALS. To complete a full period of a FODO achromat the resulting beta values at the end of the dispersion suppressor magnet must be matched by a quadrupole triplet or doublet to the symmetry point of the insertion. Triplets are necessary if small horizontal beta values are required [8]. The ALS is designed for twelve insertions (p = 12). To keep the total

length within a reasonable limit a FODO structure with four half cells per achromat has been assumed.

Several different lattices have been developed to investigate the scaling behaviour of FODO achromats. Three of them are presented here. Their characteristic parameters are given in the following table:

Optic	A	B	C
ϵ_x [radm]	4.0×10^{-9}	6.3×10^{-9}	3.9×10^{-9}
C [m]	213	232	197.5
Q_x	19.43	19.23	19.26
Q_z	10.19	10.17	11.21
ξ_x	-35.5	-29.0	-37.3
ξ_z	-20.9	-19.0	-23.3
S_x [m-2]	-17.7	-12.6	-14.5
S_z [m-2]	19.9	14.6	35.7
β_x^* [m]	3.0	2.0	2.9
β_z^* [m]	2.8	3.6	1.8
$\hat{\beta}$ [m]	3.6	3.5	2.8
$\check{\beta}$ [m]	1.0	0.68	0.64
$\hat{D}_x$ [m]	0.17	0.19	0.14
$\check{D}_x$ [m]	0.09	0.11	0.07

with

ε emittance

C circumference

Q tune value

ξ chromaticity

S integrated sextupole strength

β beta value

D dispersion value
"*" symmetry point of the insertion

Figure 4 shows structure and lattice functions of optic A. The variation of tune and beta value with momentum are drawn in Figs. 5 and 6. Figure 7 shows the maximum stable amplitude as a function of momentum found by tracking. The boundary is drawn for two different positions in the ring; the symmetry point of the insertion and the position of maximum dispersion in the FODO structure. The later diagram also includes the off - energy closed orbit. The cross points with the amplitude curve indicate the maximum allowable energy change due to Touschek scatter which is still within the dynamical aperture. Figure 8 shows the stable amplitude area for three different energies. The boundary for on momentum particles in this diagram is compared in Fig. 9 with the case where systematic and random multipole errors have been included in quadrupoles and bending magnets. Five different statistics of random errors were investigated. The results indicate that there is a considerably reduction in dynamic aperture coming from the multipole errors.

Fig. 10 shows the somewhat more relaxed optic B. Total length and correspondingly emittance have been increased. The variation of maximum stable amplitude with momentum is drawn in Fig. 11. Figure 12 shows the stable amplitude area for three different energies. The chromatic behaviour of this optic is comparable with optic A.

Structure and lattice functions of optics C are plotted in Fig. 13. To reduce the total length of the machine, the drifts between bending magnets and quadrupoles in the FODO cells have been shortened. Since they dont provide then enough space for sextupoles, it has been assumed that sextupoles are integrated in the quadrupoles. The stable amplitude area for optics C is shown in Fig. 14.

IV. Conclusion

The minimum emittance of a FODO achromat lattice has been derived, by minimizing the emittance contribution of the dispersion suppressor magnet and the bending angle distribution between dispersion suppressor magnet and bending magnet in the FODO cell. The emittance achieved by this procedure is considerably below the emittance given for a pure FODO structure. If the geometry of the FODO cell and the phase advance per cell is fixed, the resulting bending angle ratio for the optimum is independent of the number of FODO cells per achromat and the number of achromats per ring.

Acknowledgements

The author is indebted to A. Jackson and M. Cornacchia for reading the manuscript and fruitful discussions.

References

[1] The Advanced Light Source: Technical Design, LBL Pub-5111.

[2] R. Chasman, G. Green, IEEE Trans. Nucl. Sci. NS-22,1765 (1975).

[3] G. Vignola, Preliminary Design of a Dedicated 6 GeV Synchrotron Radiation Storage Ring, BNL, Upton, New York 11973.

[4] A. Jackson, A Comparison of the Chasman Green and the Triple Bend Achromat Lattices, LBL-21297, ESG-9, March 1986.

[5] A. Hutton, private communication.

[6] A. Wrulich, The Expanded Chasman Green Lattice as a Candidate for the ALS, to be published.

[7] H. Wiedemann, Design of a VUV-Radiation Source of Very High Brilliance, SSRL-ACD-Note #28.

[8] K. Kim, Optimization of Beta Function for Operation of Undulators and Wigglers, LBL-ESG Tech Note 33.

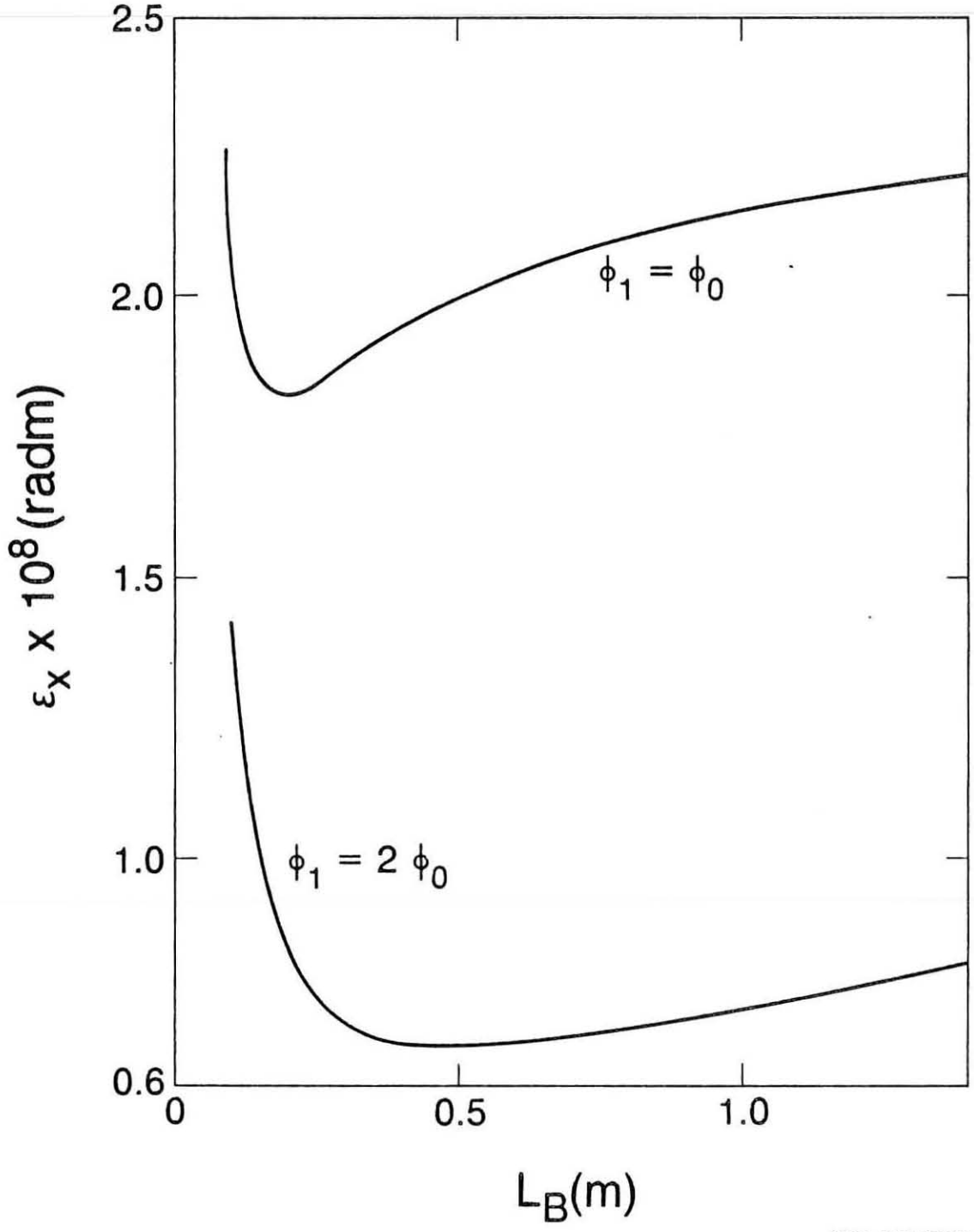

Fig. 1. Variation of emittance with length of dispersion suppressor magnet

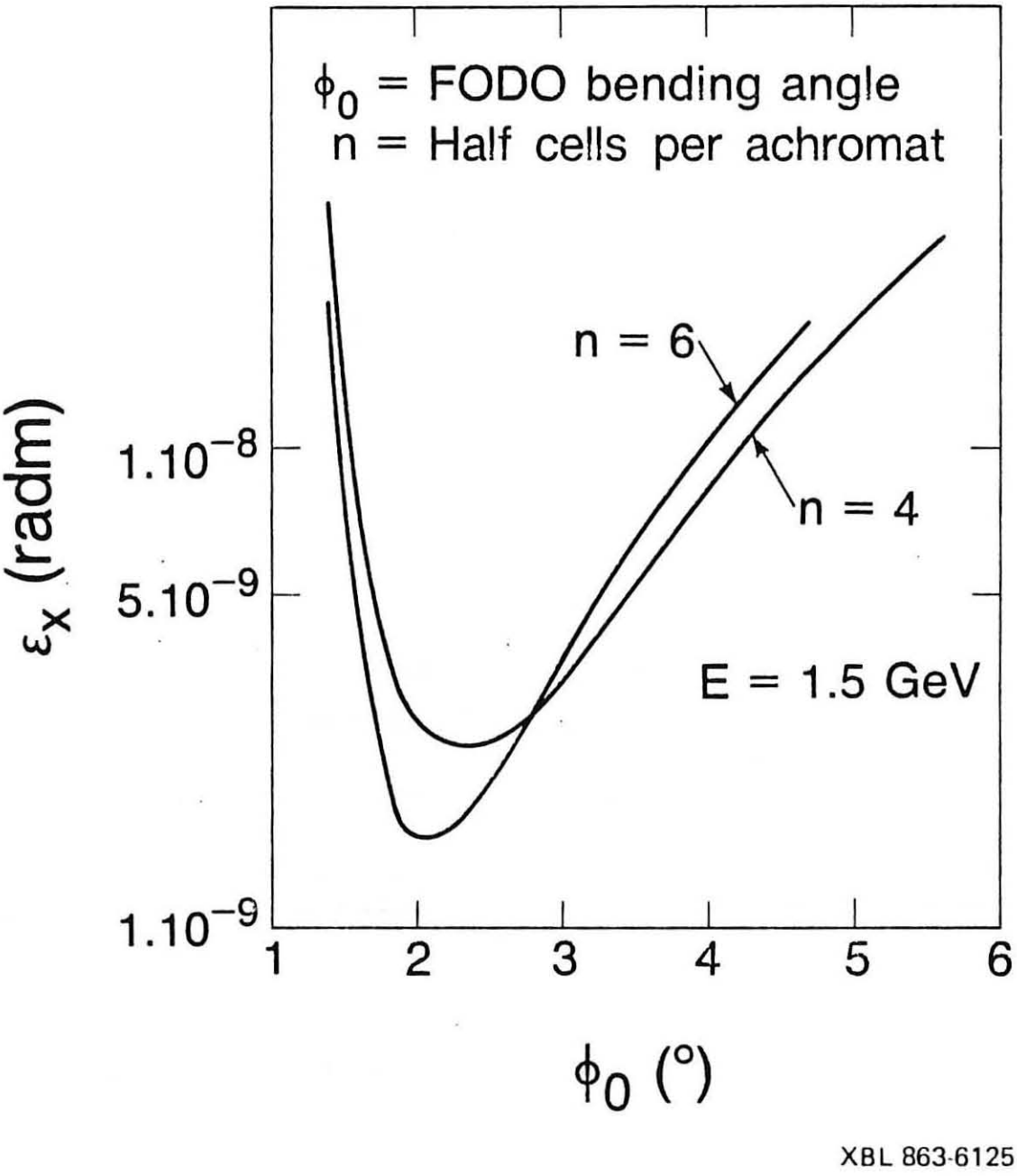

Fig. 2. Variation of emittance with bending angle distribution (12 achromats per ring)

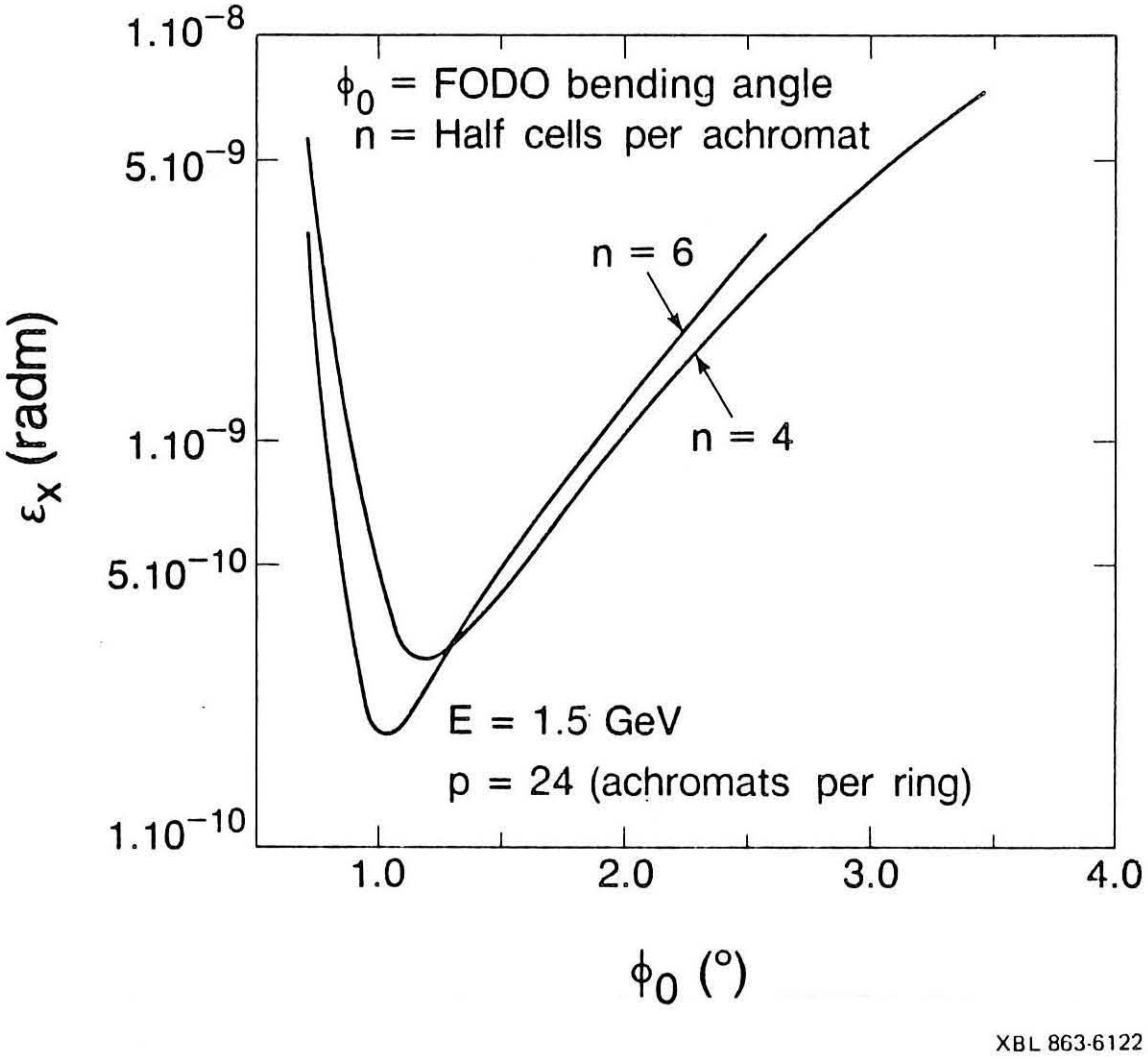

Fig. 3. Variation of emittance with bending angle distribution (24 achromats per ring)

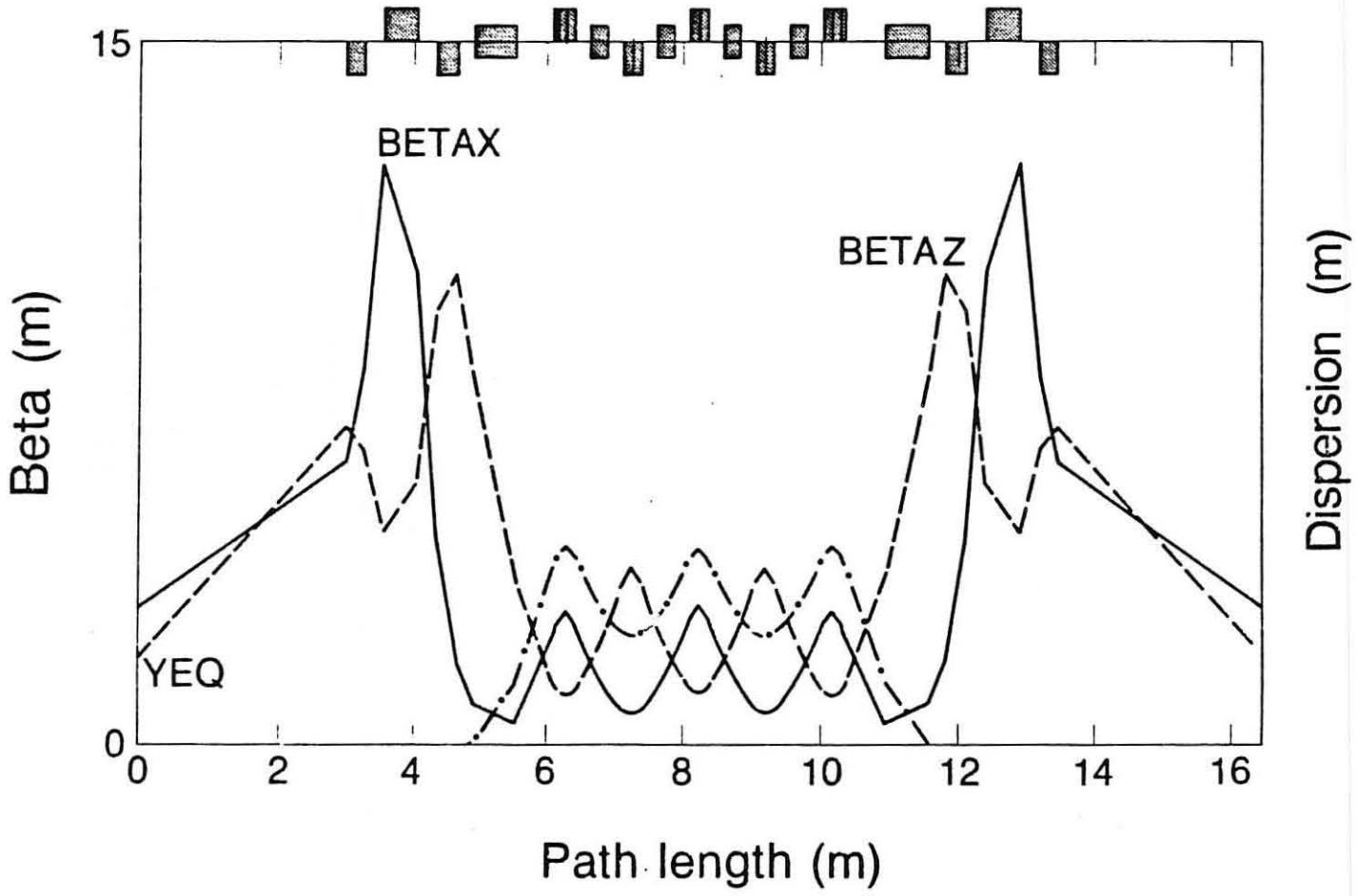

Fig. 4. Optics A - Structure and lattice functions

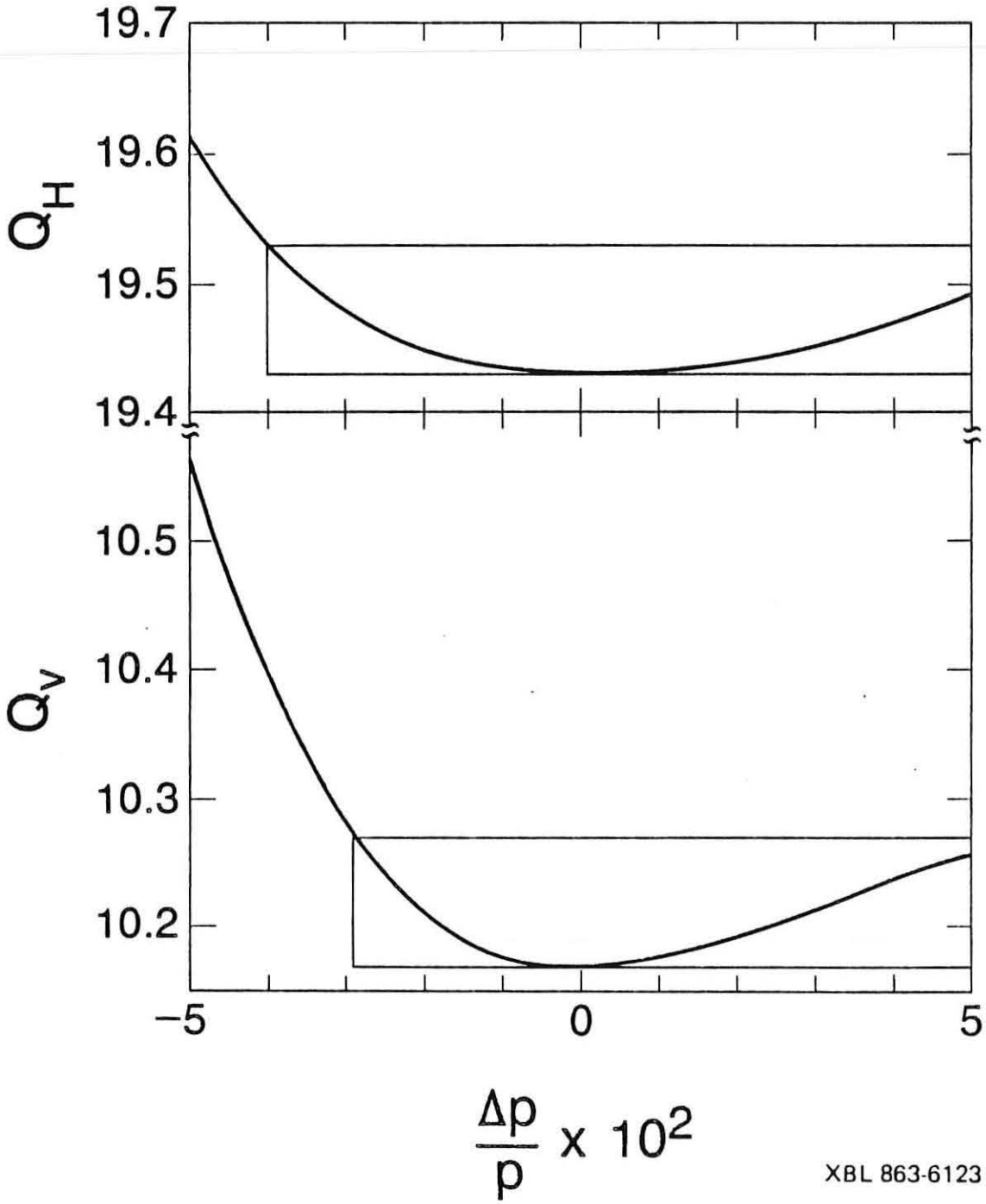

Fig. 5. Optics A - Variation of tunes with momentum

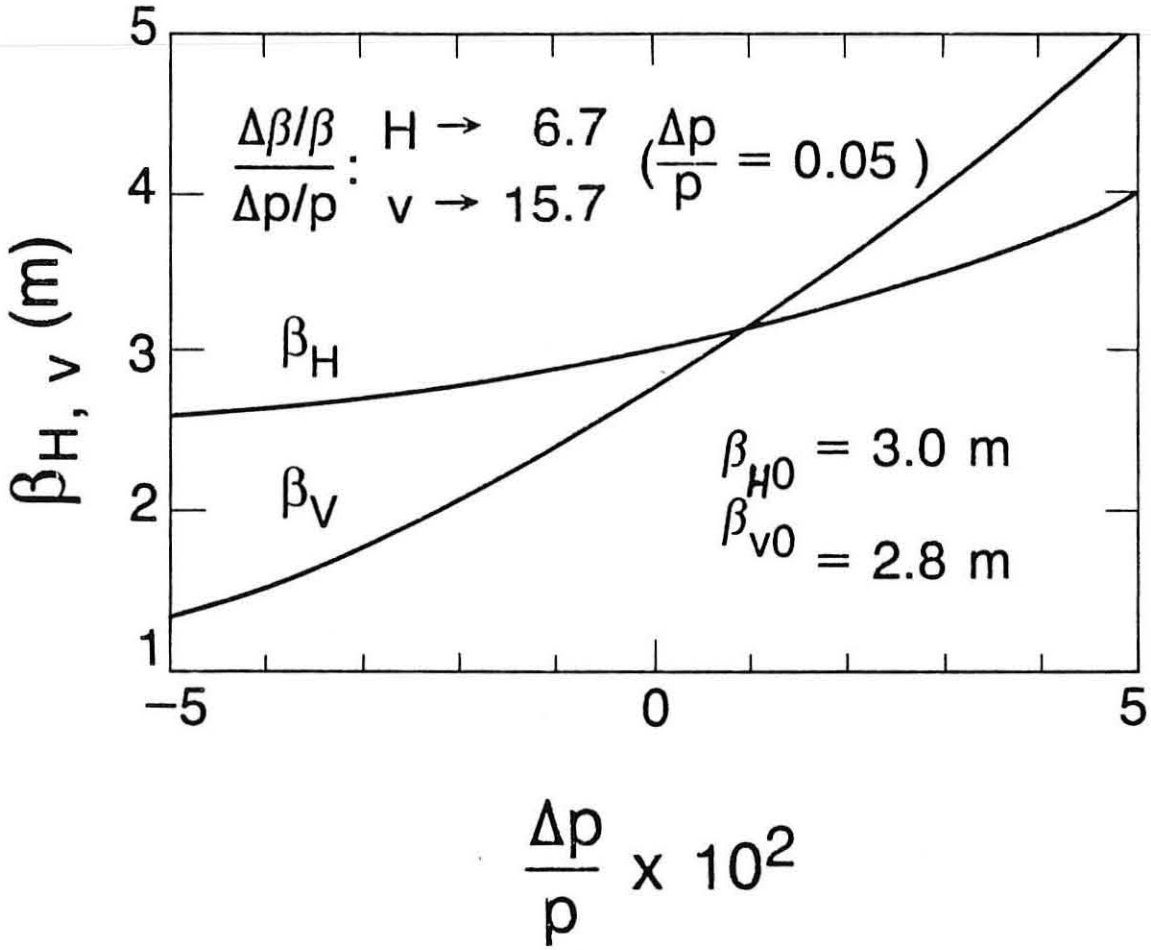

Fig. 6. Optics A - Variation of beta values with momentum

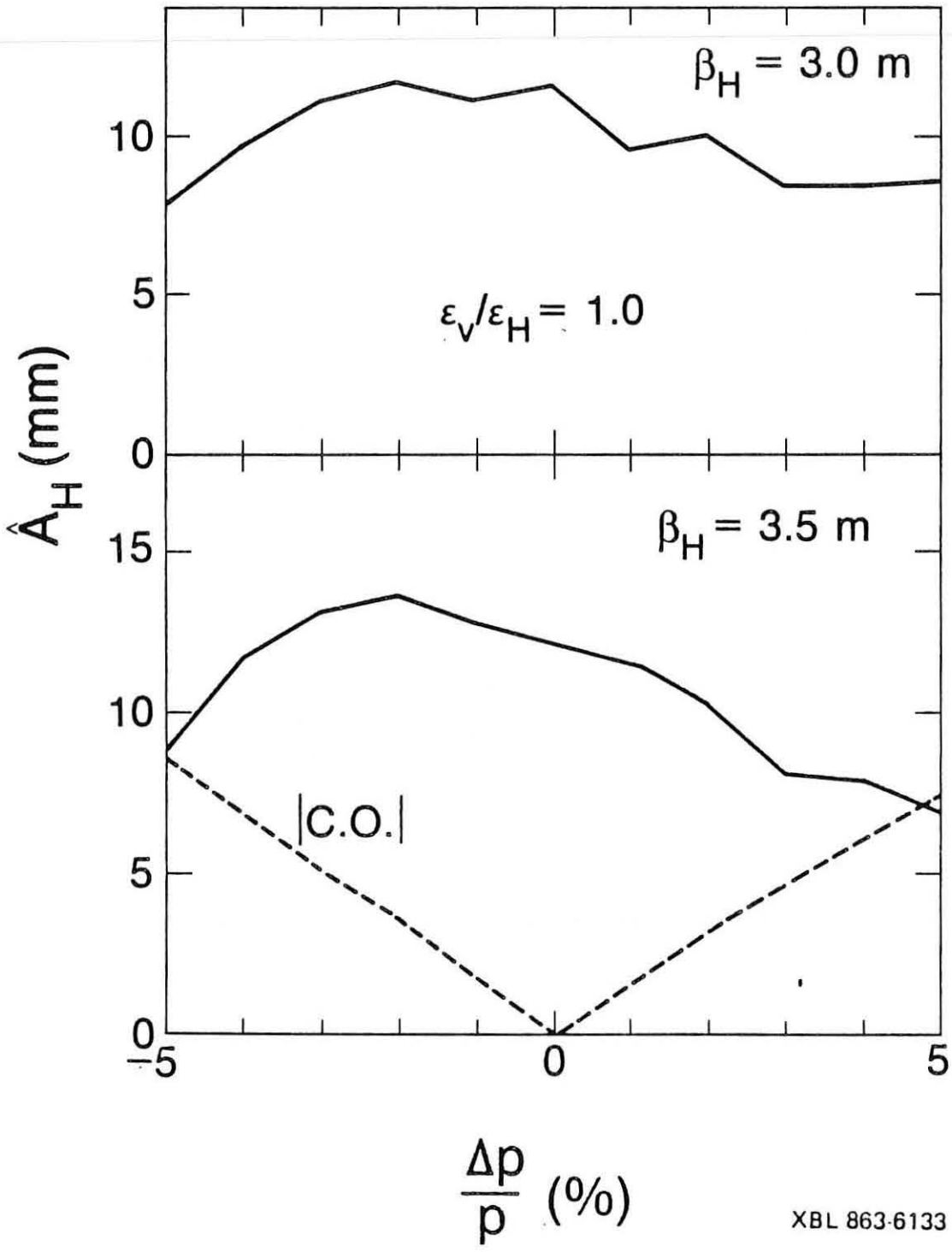

Fig. 7. Optics A - Maximum stable amplitude vs. momentum

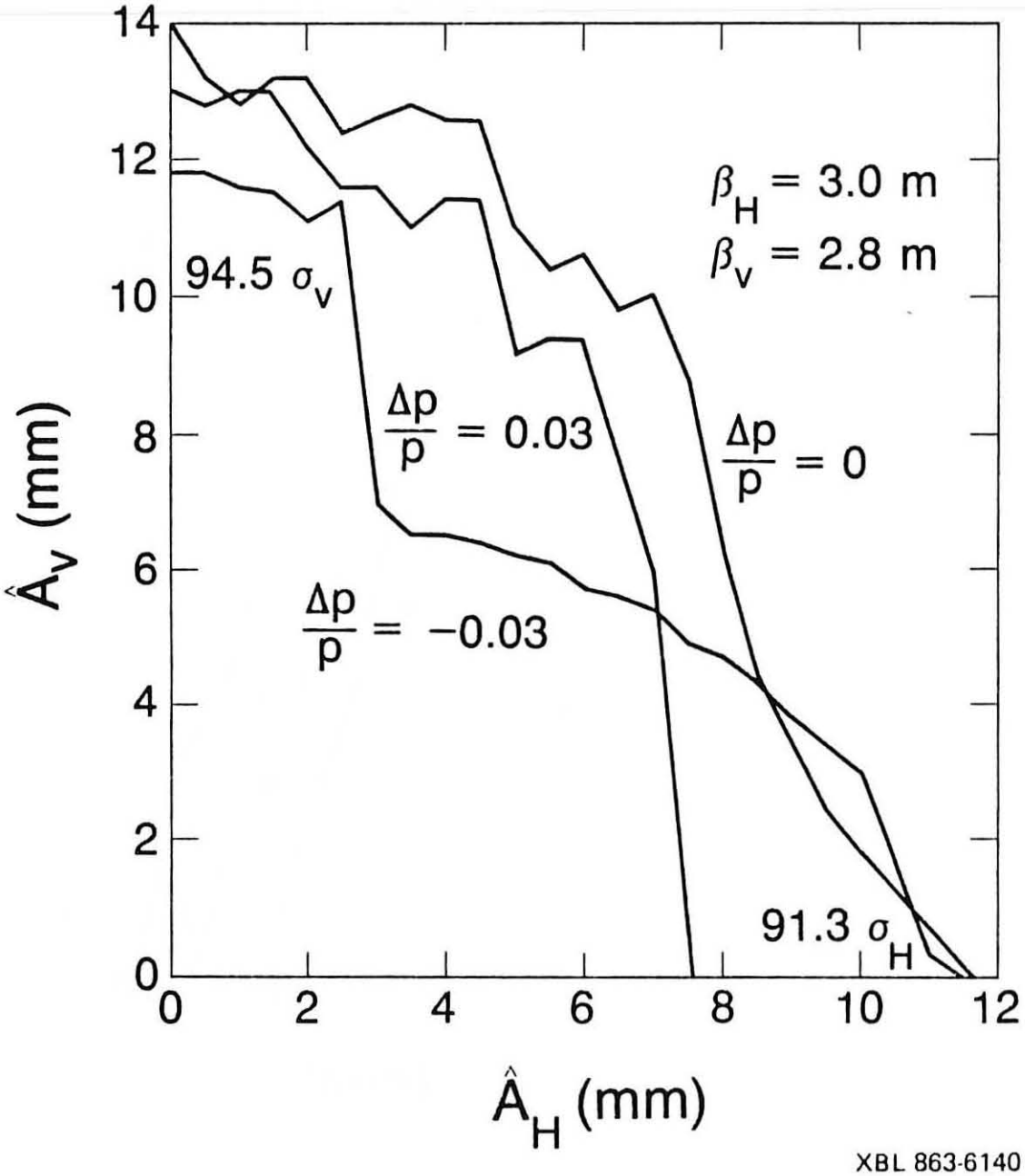

Fig. 8. Optics A - Maximum stable amplitude area

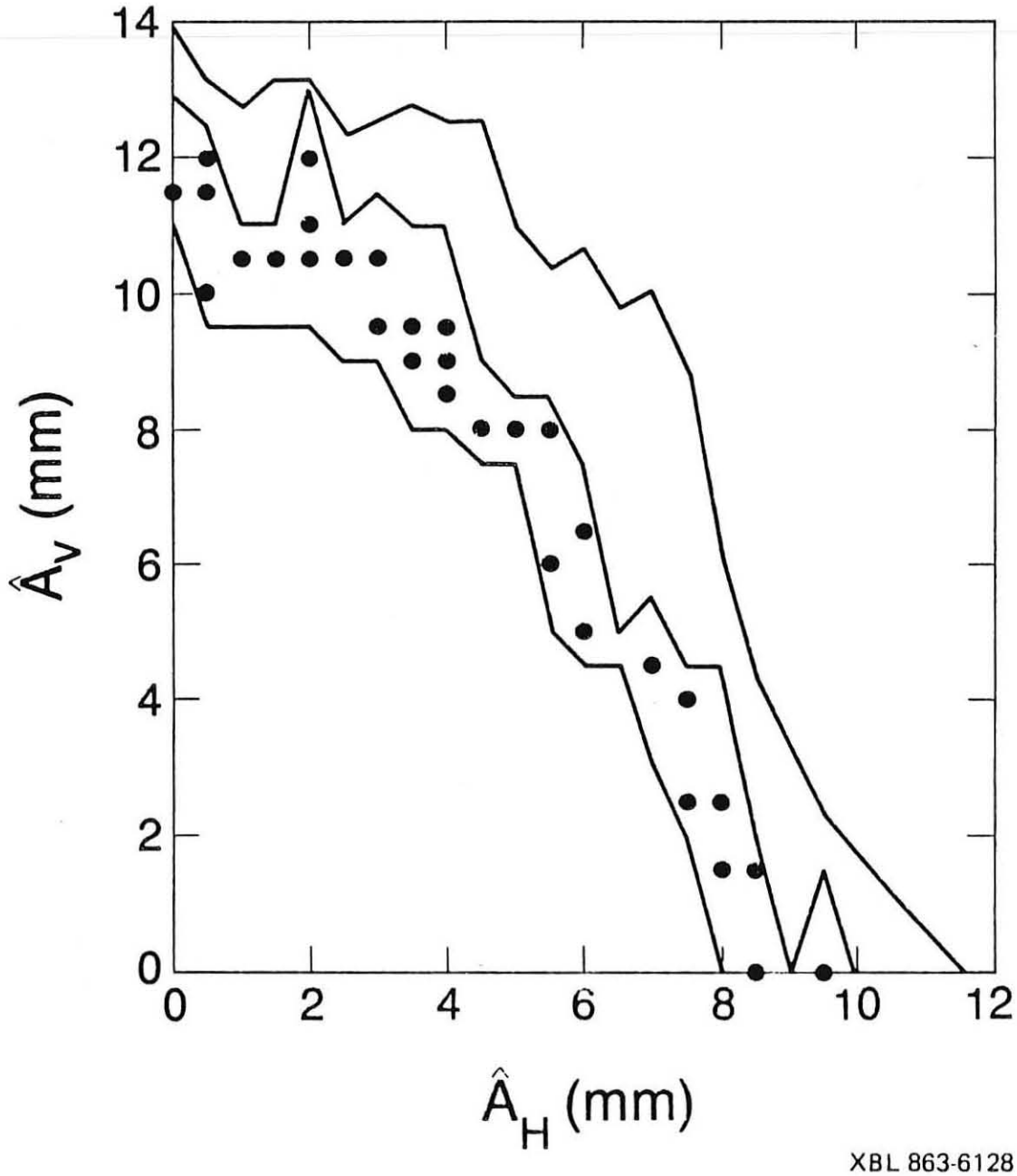

Fig. 9. Optics A - Stable amplitude area with random and systematic multipole errors

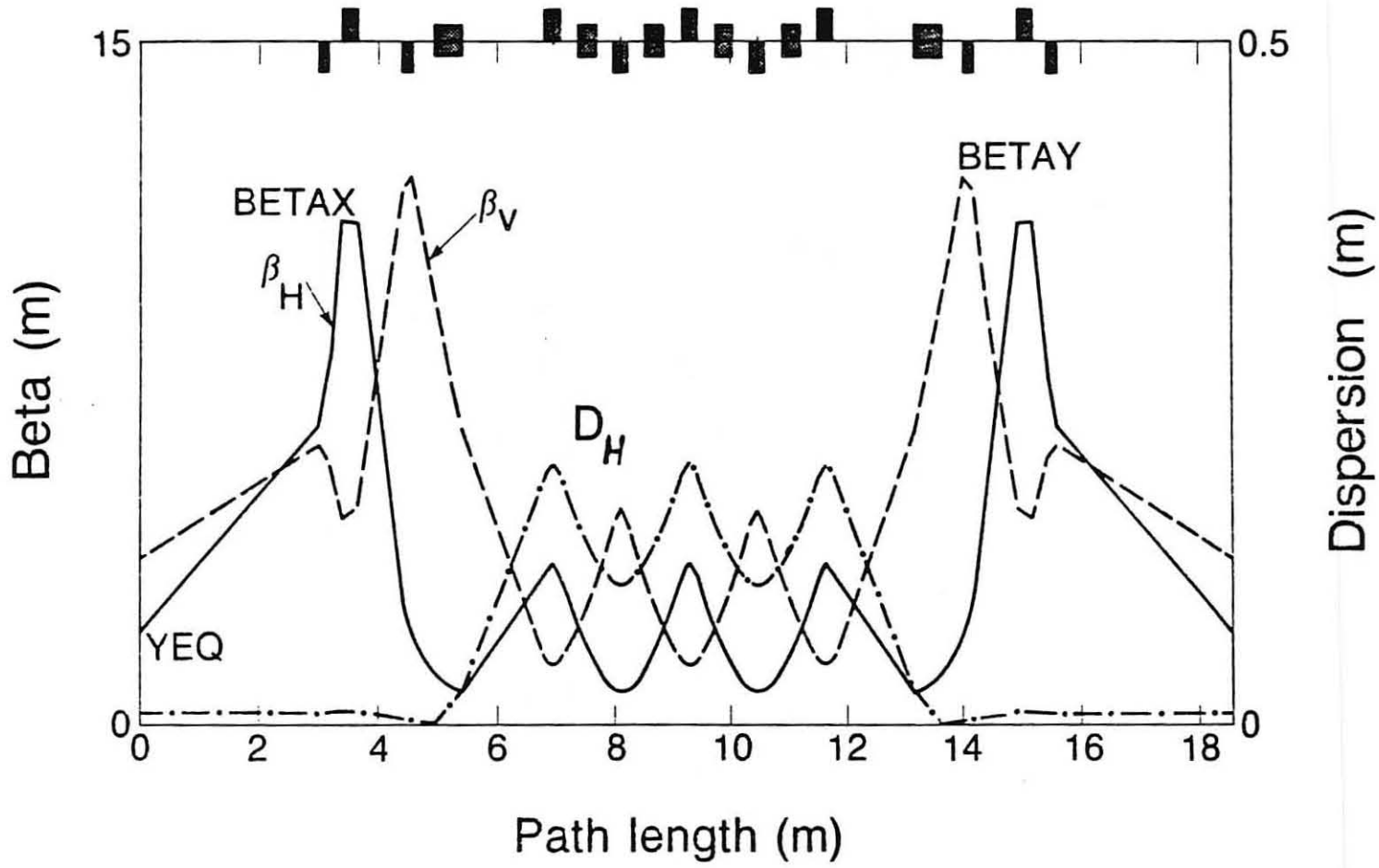

Fig. 10. Optics B - Structure and lattice functions

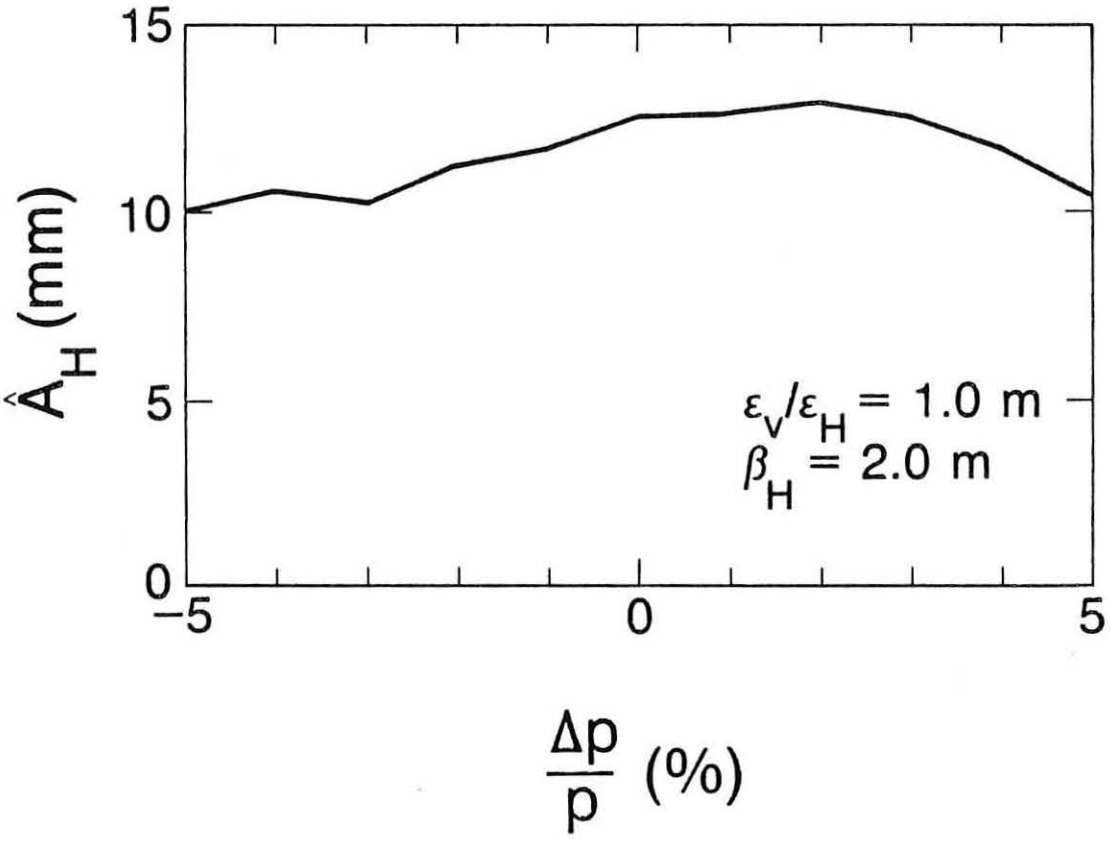

Fig. 11. Optics B - Maximum stable amplitude vs. momentum

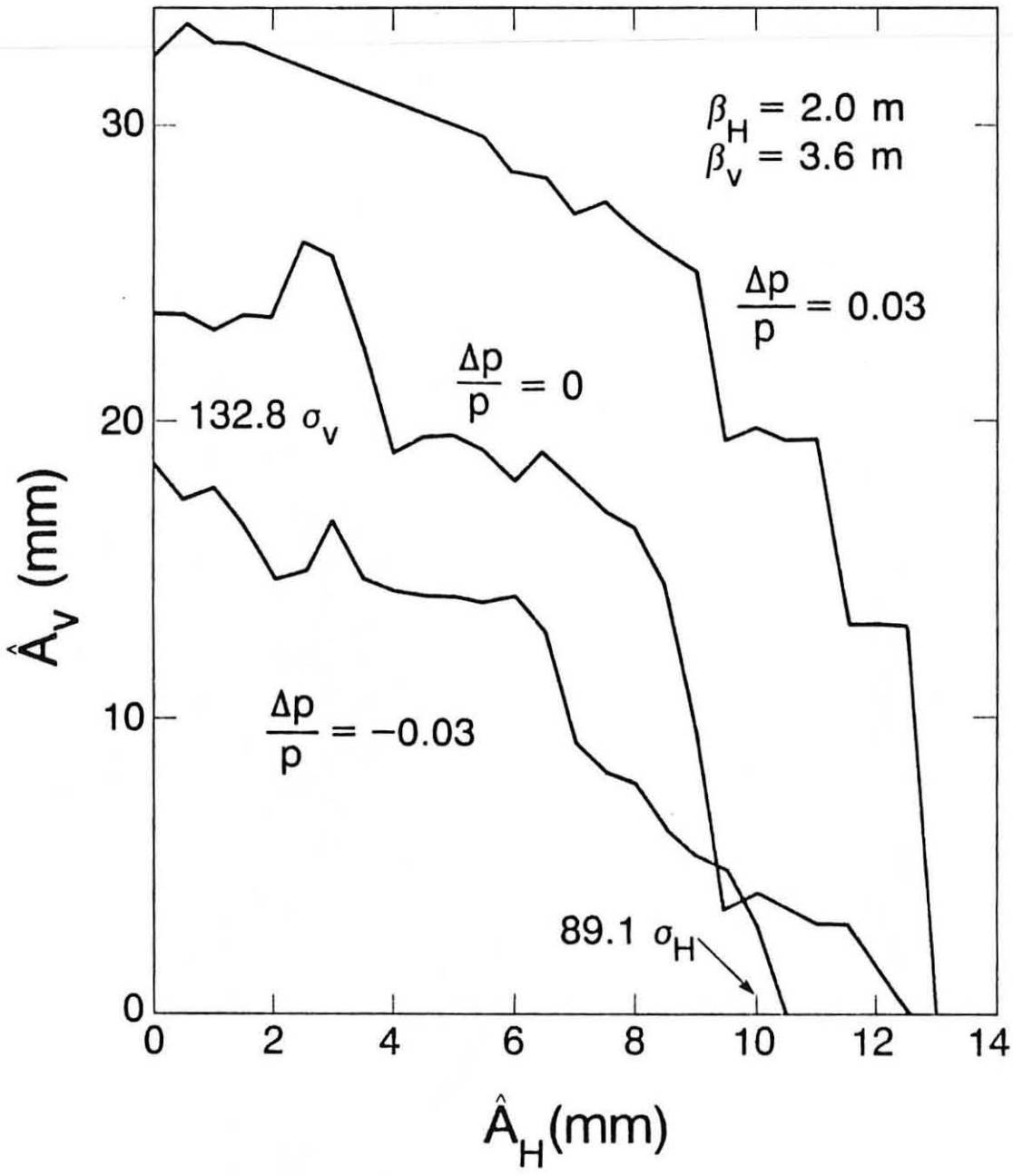

XBL 863-6132

Fig. 12. Optics B - Stable amplitude area

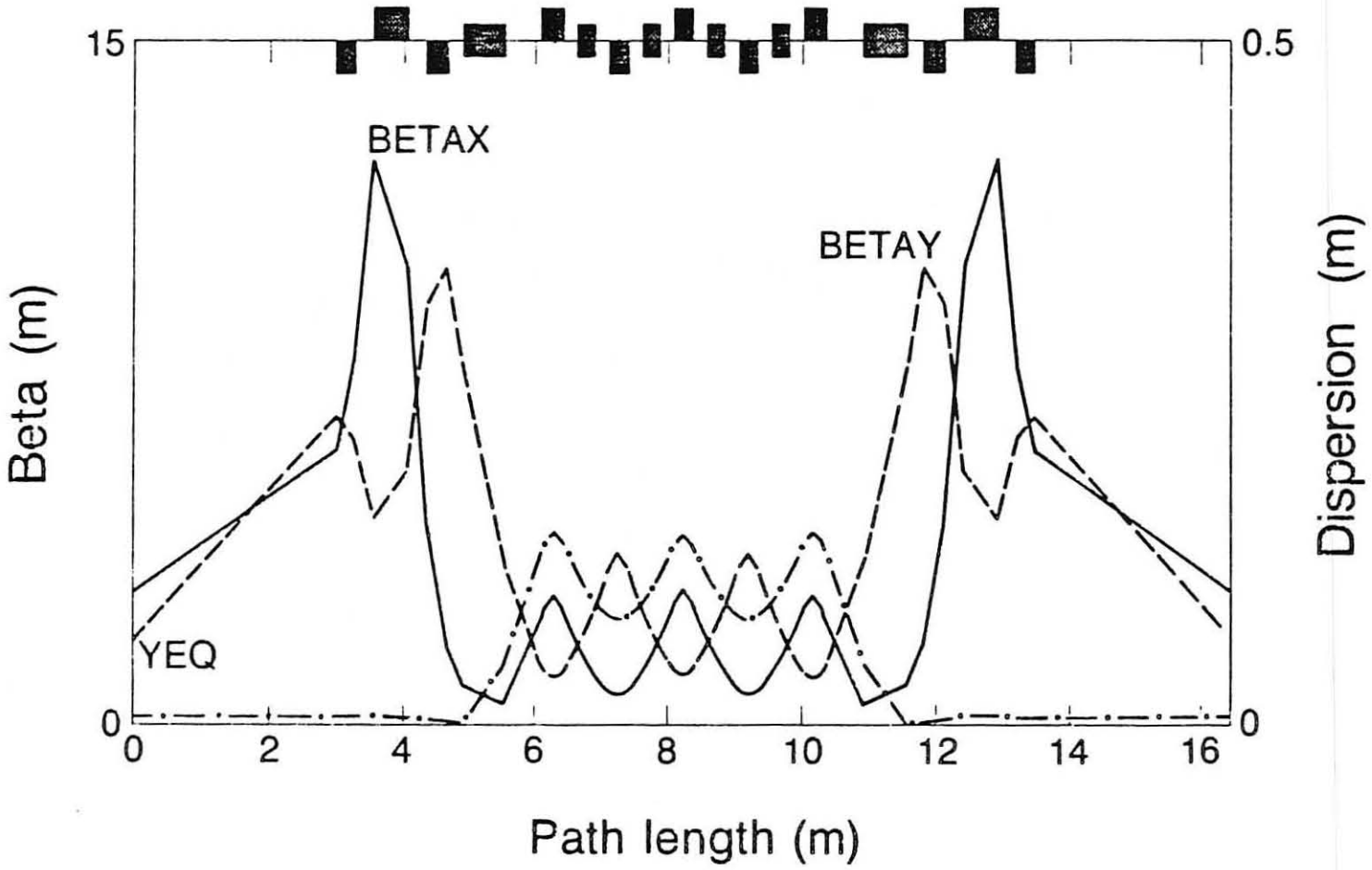

Fig. 13. Optics C - Structure and lattice functions

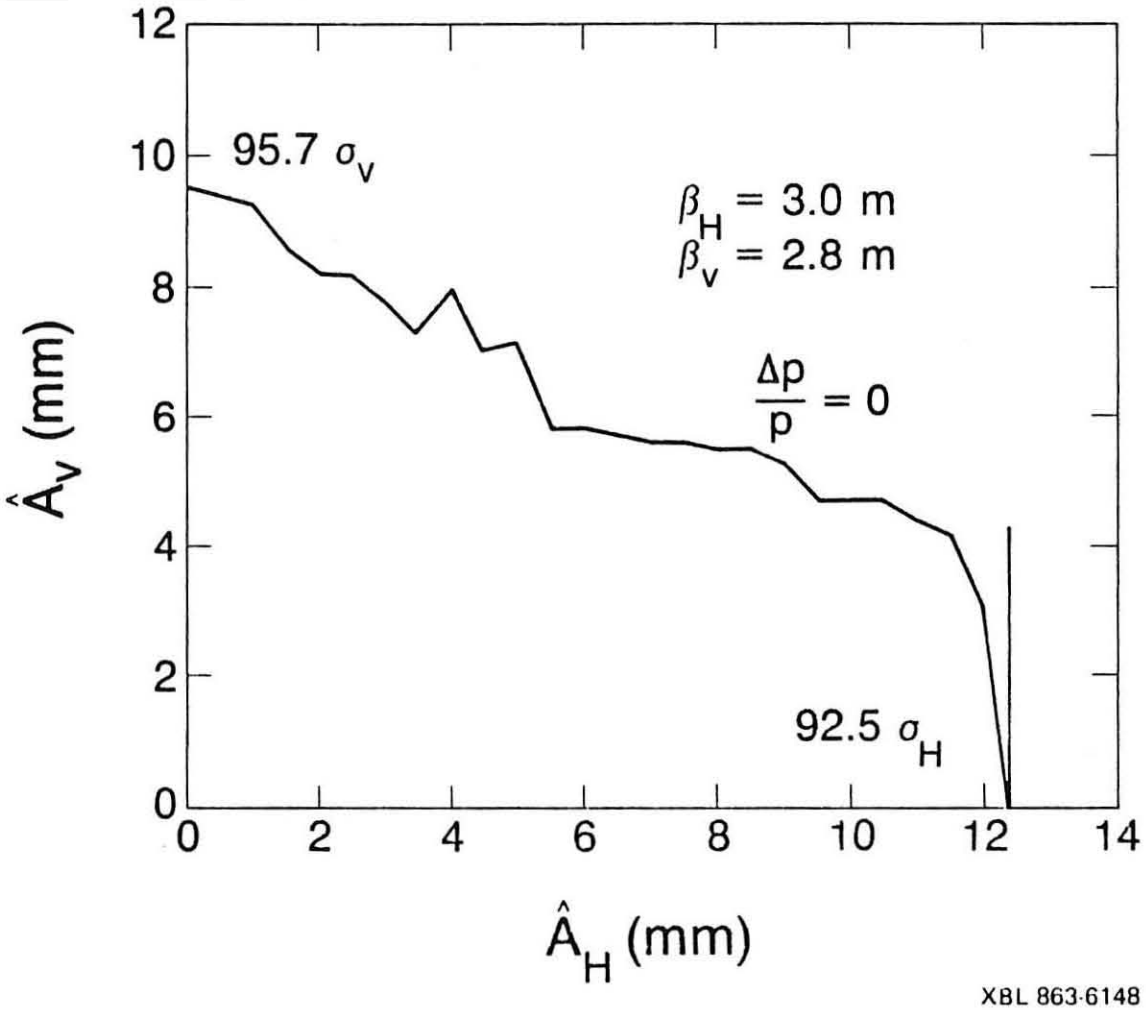

Fig. 14. Optics C - Stable amplitude area